Downscaling digital soil maps using electromagnetic induction and aerial imagery

Anders Bjørn Møller[1], Triven Koganti[1], Amélie Beucher[1], Bo V. Iversen[1], Mogens Humlekrog Greve[1]

[1]Department of Agroecology, Aarhus University, 8830 Tjele, Denmark

Correspondence to: Anders Bjørn Møller (anbm@agro.au.dk)

Abstract

Coarse-resolution soil maps at regional to national extents are often inappropriate for mapping intra-field variability. At the same time, sensor data, such as electromagnetic induction measurements and aerial imagery, can be highly useful for mapping soil properties that correlate with electrical conductivity or soil color. However, maps based on these data nearly always require calibration with local samples, as multiple factors can affect the sensor measurements. In this study, we present a method, which combines coarse-resolution, large extent soil maps with sensor data in order to improve predictions of soil properties. We test this method for predicting clay and soil organic matter contents at five agricultural fields located in Denmark. We test the method for one field at a time, using soil samples from the four other fields to predict soil properties. Results show that the method generally improves predictions over the predictions from the coarse-resolution maps, especially for soil organic matter. The method generally overestimates prediction uncertainties, a disadvantage, which will require improvements. Overall, the method is a simple, promising tool for giving a quantitative estimate of soil properties, when no local soil samples are available.

Keywords: clay, soil organic matter, electrical conductivity, remote sensing, topsoil, Denmark

1 Introduction

Over the last decades, sensor technologies have become widely applied means for mapping soil properties. In many cases, sensors have facilitated the creation of soil maps with unprecedented detail and accuracy. The resulting maps have large benefits for agricultural management practices and planning both at farm and field level (Corwin and Lesch, 2005, Magri et al., 2005). The key to the success of sensors lies in the fact that they can quickly collect large numbers of measurements, which are good proxies for soil properties. The high spatial densities of the measurements enables the creation of soil maps with similar densities.

Electromagnetic induction (EMI) is a widely applied proximal sensing technology. EMI instruments consist of a transmitter coil and one or more receiver coils. The transmitter coil induces circular eddy-current loops in the soil, and the receiver coils measure the resulting electromagnetic fields (Everett, 2013). EMI measures apparent electrical conductivity (EC_a) and is therefore useful for mapping soil properties that correlate with the electrical conductivity (EC) of the soil, including salinity, moisture, clay contents and soil organic matter (SOM) (Corwin and Lesch, 2005). Early studies focused on measurements of soil salinity (Corwin and Rhoades, 1982, Williams and Baker, 1982, Wollenhaupt et al., 1986), but later studies have proven EMI as a reliable method for mapping clay contents (Williams and Hoey, 1987, Triantafilis and Lesch, 2005, Michael Mertens et al., 2008, Heil and Schmidhalter, 2012, Doolittle and Brevik, 2014). EC_a measurements obtained with EMI are depth-weighted averages (Corwin and Lesch, 2005, Callegary et al., 2007, Heil and Schmidhalter, 2017). However, in recent years, researchers have started inverting EC_a to obtain depth-specific EC estimates. These values make it possible to map soil properties in three dimensions (Koganti et al., 2018, Khongnawang et al., 2019).

At the same time, bare soil imagery is useful for mapping SOM, as soils with high amounts of organic matter have a darker color (Ladoni et al., 2009). Some studies have employed multispectral images of soils to predict SOM (Varvel et al., 1999, Fox and Sabbagh, 2002, Roberts et al., 2010), while others have used RGB imagery (Chen et al., 2000, Achasov and Bidolakh, 2011) or even greyscale images (Gelder et al., 2011). A review by Ladoni et al. (2009) showed that infrared spectral bands had a higher correlation with SOM than bands in the visible spectrum. Likewise, Fox and Sabbagh (2002) showed that including near-infrared reflectance improved the accuracy of the predictions. However, in most cases, the red band has a higher correlation to SOM than the other visible spectral bands (Ladoni et al., 2009, Achasov and Bidolakh, 2011, Wu et al., 2018).

While EMI and bare soil imagery are useful for mapping, both techniques require local samples for calibration. Maps based on EMI require soil samples for calibration, as the relationships with soil properties are often site-specific, and factors that vary over short time intervals, such as temperature and water contents, can influence the measurements (Corwin and Lesch, 2005, Heil and Schmidhalter, 2017). Likewise, it is difficult to establish universal models linking SOM to soil color, as moisture, vegetation, crop residues and tillage affect colors in the images (Ladoni et al., 2009, Roberts et al., 2010).

Unlike EMI and aerial imagery, large-extent soil maps often do not account for intra-field variability of soil properties. In many cases, this is due to their coarse resolution. However, even when the resolution is nominally high, other factors, such as the sampling strategy can limit the ability to map soil properties within fields. For example, Adhikari et al. (2013) and Adhikari et al. (2014) mapped soil texture and SOM, respectively, at 30.4 m resolution for Denmark, using legacy soil observations (Madsen and Jensen, 1985, Madsen et al., 1992, Greve et al., 2014). The majority of the soil samples used by Adhikari et al. (2013) and Adhikari et al. (2014) originated from a large mapping effort carried out in the 1970s (Madsen et al., 1992). In this effort, surveyors used judgment sampling to select representative areas within fields. Furthermore, the samples were all composites of 25 to 30 subsamples from within areas of about 5000 m^2. Therefore, the samples from this effort have limited use for mapping intra-field variability in soil properties.

In short, sensors and large extent soil maps have contrasting capabilities. On the one hand, sensors can account for intra-field variability but need local samples for calibration. On the other hand, coarse-resolution large-extent soil maps may well represent the mean of a soil property within a field, but fail to account for intra-field variability.

In this study, we propose an approach that combines sensor data with coarse-resolution large-extent soil maps. The aim is to map clay and SOM contents for agricultural fields without using local soil samples by combining predictions from coarse-resolution soil maps with regression models that relate variation in the soil properties with sensor data. Firstly, we will use median values from the coarse-resolution rasters within the fields. We will then modify these values with models that account for deviations from the median, using deviations from the sensor data medians as explanatory variables.

The usefulness of this approach relies on the following assumptions:

1. The clay and SOM contents in the coarse-resolution rasters represent accurately the median values within the agricultural fields.
2. Variations in clay contents within the fields are the main driver for variation in EC.
3. Variations in SOM contents within the fields are the main driver for variation in soil brightness (SB) in aerial images.

We will test the proposed approach for five agricultural fields located in Denmark. We hypothesize that (1) the median values modified by sensor-data will predict clay and SOM contents more accurately than the coarse-resolution rasters. We also hypothesize that (2) it is possible to estimate accurately the uncertainties associated with the method. Lastly, we hypothesize that (3) the fulfilment of the three assumptions listed above will be the deciding criterion for the accuracy of the predictions.

2 Materials and methods

2.1 Study areas

The five fields used in this study are located in Denmark in northern Europe (Figure 1).

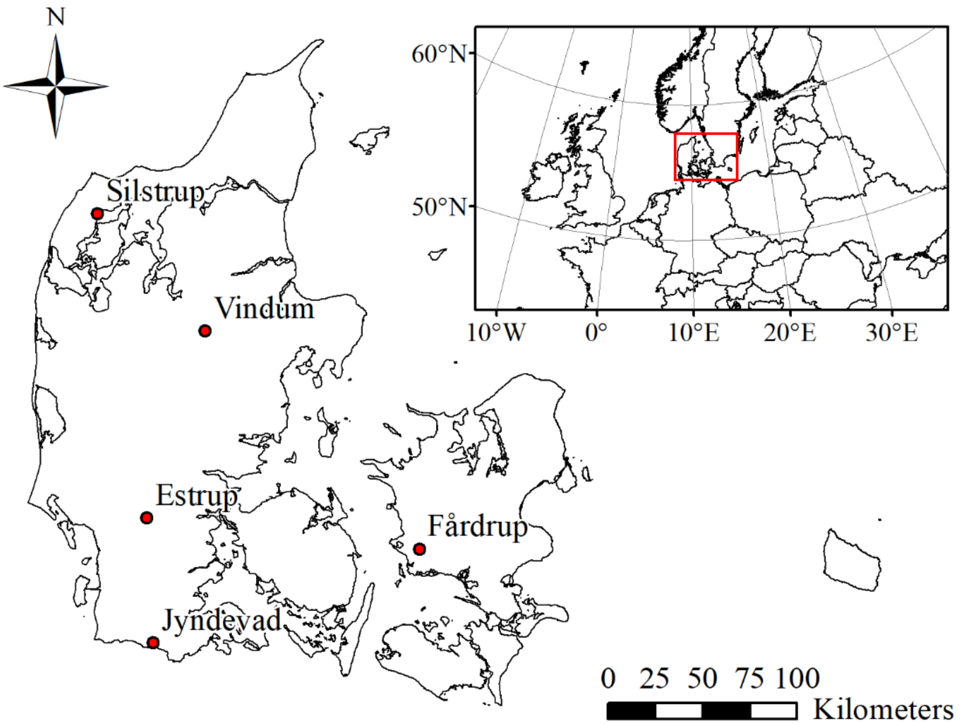

Figure 1: Location of Denmark in Europe and the locations of the five fields used in the study.

2.1.1 Estrup

The field at Estrup (Figure 2A) has an area of 1.3 ha and lies on a hill, 56 to 58 m above sea level in a Saalian moraine landscape. The topography is mildly undulating and slopes slightly (1.1%) towards the northeast. The dominant surface geology within the field is clay till, while some small areas contain glaciofluvial sand. The soils within the field include Abruptic Argiudolls, Aquic Argiudolls and Fragiaquic Glossudalfs (Lindhardt et al., 2001).

2.1.2 Fårdrup

The field at Fårdrup (Figure 2B) has an area of 2.4 ha and lies near the top of a hill, 30 to 33 m above sea level in a Weichselian moraine landscape. The field generally slopes towards the west with a mean gradient of approximately 1.7%. Clay and sand till are the dominant surface geologies, with smaller parties of glaciofluvial sand. The soils within the field include Haplic Vermiudolls, Oxyaquic Hapludolls and Oxyaquic Argiudolls (Lindhardt et al., 2001).

2.1.3 Jyndevad

The field at Jyndevad (Figure 2C) has an area of 2.4 ha and lies in a glacial outwash plain, 14 to 15 m above sea level. The field generally slopes towards the southwest with a mean gradient of 1.3%. Glaciofluvial sand is the dominant surface geology. The soils within the field are Typic Haplorthods (Lindhardt et al., 2001).

2.1.4 Silstrup

The field at Silstrup (Figure 2D) has an area of 1.7 ha and lies at 41 to 45 m above sea level, close to the top of a hill in a terminal moraine formed by a late-Weichselian ice advance from the north. The field slopes towards the north with a mean gradient of 2.2%. The dominant surface geology is clay till. The soils within the field are Alfic Argiudolls and Typic Hapludolls (Lindhardt et al., 2001).

2.1.5 Vindum

The field at Vindum (Figure 2E) has an area of 11.7 ha and lies 55 to 66 m above sea level in a Weichselian kettled moraine landscape. The landscape is undulating with a depression near the center of the field. Surface geologies include clay till, glaciofluvial sand and peat (Olesen and Simmelsgaard, 1995). Based on data from the Danish Soil Profile Database (Madsen and Jensen, 1985), soil types within the field include Alfisols, Inceptisols, Mollisols and Histosols. In most cases, they are Arenic Oxyaquic Hapludalfs, Mollic Oxyaquic Hapludalfs or Oxyaquic Humudepts. The depression near the center of the field contains most of the Histosols (Møller et al., 2019, Pouladi et al., 2019). Greve and Greve (2004) showed a high correlation between clay contents and EC_a within the field.

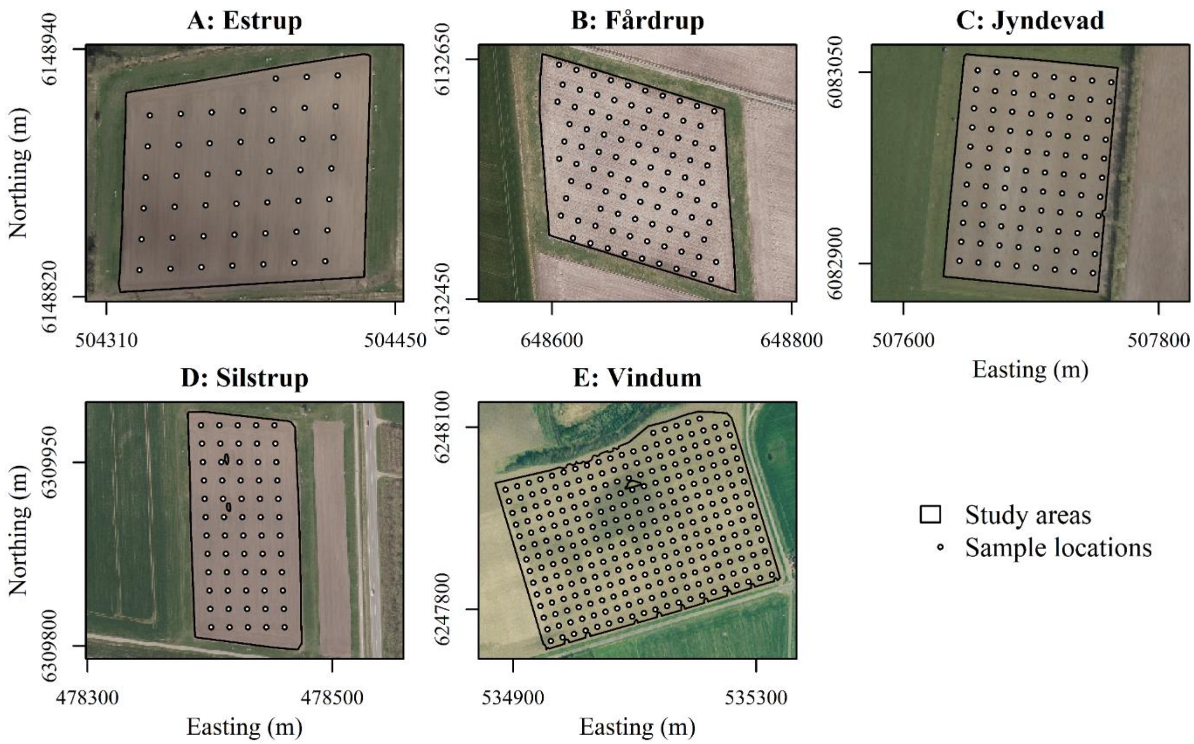

Figure 2: Maps of the five fields used in the study, including field boundaries and sampling locations. Backgrounds show orthophotos from the spring 2017 (A, B, C, D) and from the spring 2006 (E) (Agency for Data Supply and Efficiency, 2019). The axes show coordinates for UTM zone 32N, ETRS 1989.

2.2 Input data

2.2.1 Soil samples

We used soil samples extracted from the depth interval 0 to 25 cm for all five fields. At Estrup, the samples were located in a rhombic grid, while in the other fields a square grid was in use (Figure 2). At Vindum, the grid spacing was 20 m, while the other fields had 15-m grid spacings. Table 1 gives the number of samples extracted from each field, and Figure 2 gives an overview of the grid sampling design of the different fields.

The soil samples were dried and crushed to pass through a 2 mm sieve. Particle size distribution was determined by sieving and hydrometric methods (Gee and Bauder, 1986), while soil organic carbon content was determined by combustion in a LECO induction furnace and converted to SOM by multiplication with 1.72 (Tabatabai and Bremner, 1970).

Adhikari et al. (2013) and Adhikari et al. (2014) did not use the soil observations from the five fields when producing the coarse-resolution maps of clay and SOM contents.

2.2.2 EMI surveys

We used EC_a measurements from EMI surveys conducted with a DUALEM-21S sensor (Dualem Inc., Milton, ON, Canada) in the years 2010 to 2012 at the five fields. Table 1 lists the dates of the surveys for each field.

The DUALEM-21S is a single-transmitter multi-receiver electromagnetic induction (EMI) instrument operating at a frequency of 9 kHz. It has a transmitter coil located at one end. Two pairs of receiver coils in horizontal coplanar (HCP) and perpendicular (PRP) orientations share the transmitter coil. For the HCP configurations, the transmitter-receiver separation distances are 1 and 2 m, and for the PRP configurations, they are 1.1 and 2.1 m respectively. The quadrature-phase and in-phase signal responses of the EMI sensor are representative of the EC_a and the magnetic susceptibility of the soil (McNeill, 1980). At low induction numbers, the depth sensitivity of EC_a measurements is approximately a function of coil spacing (S) and array orientation. Furthermore, the depth of exploration can be defined as the depth at which the signal accumulates 70% of its total sensitivity (McNeill, 1980). Hence, the depth of exploration for HCP and PRP arrays are 1.6 S and 0.5 S, respectively when the instrument is placed on the ground (Dualem Inc, 2007). As such, the 1.1 m and 2.1 m PRP configurations provide measures of EC_a for soil volumes reaching depths of 0.5 and 1.0 m, whereas the 1 m and 2 m HCP configurations provide EC_a to depths of 1.6 and 3.2 m, respectively. The actual depth of investigation can vary significantly depending on the true EC. This is because the low induction number approximation is no longer valid in highly conductive (> 100 mS m^{-1}) conditions, and the corresponding measurement depth will be smaller (Christiansen et al., 2016).

The instrument was mounted on a sled (at a height of 0.3 m above the ground) attached to an ATV, with real-time data georeferencing using an RTK GPS. Dedicated data processing was performed using Aarhus Workbench software (Auken et al., 2009) by removing the negative EC_a values and noise due to anthropogenic coupling (metal cables, field monitoring installations etc.). Afterwards, the data were corrected for the offset between GPS and the individual channels. We further improved the signal-to-noise ratio (SNR) by averaging the data, choosing an appropriate sounding distance and running mean width. We inverted EC_a with a quasi-3D spatially constrained inversion algorithm (Viezzoli et al., 2008, Auken et al., 2015) using a ten-layer model to estimate the average EC of the topsoil (0 – 30 cm). Afterwards, we interpolated point values of topsoil EC to a 1.6 m raster using ordinary kriging with an exponential variogram.

Table 1: Overview of the fields used in the study, including their area, number of samples, the date of the EMI survey and the dates of the orthophotos, with the number of orthophotos for each field in parentheses.

Field	**Area (ha)**	**Samples (n)**	**EMI survey (date)**	**Orthophotos [dates (n)]**
Estrup	1.3	45	2011-09-05	Spring 2016, spring 2017, spring 2018 (3)
Fårdrup	2.4	95	2011-07-28	Spring 2012, spring 2016, spring 2017, spring 2018 (4)
Jyndevad	2.4	88	2012-05-02	Summer 2010, summer 2012, spring 2017 (3)
Silstrup	1.7	65	2011-05-16	Spring 2015, spring 2016, spring 2017 (3)
Vindum	11.7	307	2010-04-17	Spring 2006, spring 2018 (2)

2.2.3 Aerial images

We obtained two to four bare-soil orthophotos for each field from the years 2006 to 2018. We used orthophotos from the GeoDanmark webservice (Agency for Data Supply and Efficiency, 2019). Table 1 lists the dates of the images obtained for each field. Some of the images contained an infrared band in addition to RGB data. However, we omitted the infrared data, as this allowed us to use more images. Furthermore, aerial images often only contain RGB data, and by omitting the infrared band, we aimed to make our results more generally applicable. We stored the images as RGB rasters and manually cropped out shadows and non-soil features. The resolutions of the images ranged from 10 to 50 cm. We extracted SB in the red band for each image and then aggregated the rasters to a common 1.6 m resolution. We then averaged SB across the images for each field in order to reduce effects from individual images.

2.2.4 Coarse resolution maps

We used coarse-resolution maps of clay and SOM contents produced by Adhikari et al. (2013) and Adhikari et al. (2014), respectively. The authors of these studies produced these maps at 30.4 m-resolution for all of Denmark, using Cubist regression models with kriged residuals. The authors produced predictions for several depth intervals, but we used only the predictions for the depth interval 0 to 30 cm.

2.3 Centered measurements

A preliminary analysis showed a correlation between the standard deviation (SD) of EC within each field and their median ($R^2 = 0.85$, n = 5, $p < 0.05$). However, there was no correlation between median EC and median clay contents from the coarse-resolution map ($\widetilde{clay}_{CR,i}$, $p > 0.05$, n = 5). This suggested to us that EC variation within each field was proportional to the median EC, but not proportional to variation in clay contents. We therefore scaled EC for each field using the median clay contents from the coarse-resolution map in order to make variation proportional to the predicted clay contents:

$$EC_{SC} = EC * \frac{\widetilde{clay}_{CR,i}}{\widetilde{EC}_i} \qquad [1]$$

where EC_{SC} is scaled EC, $\widetilde{clay}_{CR,i}$ is the median clay content from the coarse-resolution map for field *i*, and $\widetilde{EC}_i$ is median EC for field *i*.

Furthermore, our approach relies on the assumption that intra field variations in EC and SB reflect variation in clay contents and SOM, respectively. We therefore centered clay and SOM contents, EC_{SC} and SB for each field using the median of each variable. We used the median, as it is robust towards outliers. Furthermore, we transformed SOM contents by natural logarithm:

$$clay_C = clay_O - \widetilde{clay}_{O,i} \qquad [2]$$

$$\ln(SOM)_C = \ln(SOM_O) - \ln(\widetilde{SOM})_{O,i} \qquad [3]$$

$$EC_C = EC_{SC} - \widetilde{EC_{SC,\imath}} \qquad [4]$$

$$SB_C = SB - \widetilde{SB_{\imath}} \qquad [5]$$

where $_C$ signifies centered values, $_O$ signified observed values.

2.4 Prediction of clay and SOM contents

We trained regression models to account for the relationship between $clay_c$ and EC_c and between $ln(SOM_c)$ and SB_c. We used two forms of regression: linear regression (LR) and local regression (LOESS) (Cleveland et al., 1992). One the one hand, we included LR for its relative robustness and mathematical simplicity. On the other hand, we included LOESS for its ability to account for non-linear relationships between variables. In our study, each LOESS model combined several locally fitted LR models, each spanning 67% of the data.

We tested the approach for one field at a time, using leave-site-out (LSO) cross validation. For each field, we trained models from the centered values of the four other fields. We then used these models to predict $clay_c$ and $ln(SOM_c)$ for the field that was left out and added the medians from the coarse-resolution maps. We also transformed SOM estimates from logarithmic to a linear scale.

$$\widehat{clay} = \widehat{clay}_C + \widetilde{clay_{CR,\imath}} \qquad [6]$$

$$\widehat{SOM} = e^{\ln(\widehat{SOM})_C + \ln(\widetilde{SOM_{CR,\imath}})} \qquad [7]$$

where ^ indicates predicted values, and $_{CR}$ indicates values from the coarse-resolution maps.

We calculated uncertainties for the predictions as 95% prediction intervals. First, we calculated the standard error of the predictions by adding the standard error of the median values in the coarse map to the prediction standard error of the model:

$$SE_p = \sqrt{{SE_{fit}}^2 + {SE_{res}}^2} + SE_{CR,i} \qquad [8]$$

where SE_p is the standard error of the predictions, SE_{fit} is the standard error of the model fit, SE_{res} is the standard error of the model residuals, and $SE_{CR,i}$ is the standard error of the median values in the coarse-resolution map for the fields used in the model.

We then calculated the boundaries of the prediction interval by adding and subtracting standard error multiplied by the quantile of Student's t-distribution from the predicted value.

$$PI_{0.95} = \hat{y} \pm SE_p * Q(p = 0.975, v = n) \qquad [9]$$

where $\hat{y}$ the predicted soil property (clay (%) or ln[SOM (%)]), Q is the quantile of Student's t-distribution, p is the probability, and v is the degrees of freedom n. For LR, n is a constant, but for LOESS, n varies for prediction points.

As we produced predictions for each field without using local samples, we assessed the accuracies of the predictions using all samples for each field. We calculated accuracies as Pearson's R^2 and root mean square error (RMSE). We also calculated the proportion of soil observations that were within the 95% prediction interval.

Furthermore, for comparison, we calculated accuracies for the coarse-resolution maps and for regression using local samples. We assessed the accuracies of regression with local samples by leave-one(-sample)-out (LOO) cross validation.

To compare the RMSE of the LSO predictions with the RMSEs of predictions with local samples and of the coarse-resolution maps, we also calculated for each field the relative improvements (RI) for clay and SOM predictions, respectively:

$$RI_i = \frac{RMSE_{LSO,i} - RMSE_{CR,i}}{RMSE_{LOO,i} - RMSE_{CR,i}} \qquad [10]$$

where RI_i is the relative improvement for field i (%), $RMSE_{LSO,i}$ is the RMSE of LSO predictions for field i, $RMSE_{CR,i}$ is RMSE for the coarse-resolution map for field i, and $RMSE_{LOO,i}$ is the lowest RMSE for predictions with local samples (LR or LOESS), calculated using leave-one(-sample)-out (LOO) cross-validation for field i.

RI = 0% indicates RMSE on par with the coarse-resolution map, while RI = 100% indicates RMSE on par with regression using local samples.

3 Results and discussion

3.1 Comparison with coarse-resolution maps

The observed medians for clay and ln[SOM] generally showed linear relationships with the medians in the coarse-resolution maps (Figure 3). However, the observed median clay contents at Silstrup and Vindum were visibly lower than the medians in the coarse-resolution map (2.3 and 2.2% lower, respectively). Meanwhile, the coarse-resolution SOM map overstated values for fields with low SOM contents and understated values for fields with high SOM contents. In the extremes, the mapped median SOM content was 1.3 times higher than the observed median at Vindum, and the mapped median was 1.3 times lower than the observed median at Estrup. One should expect these deviations to cause biases in the predictions.

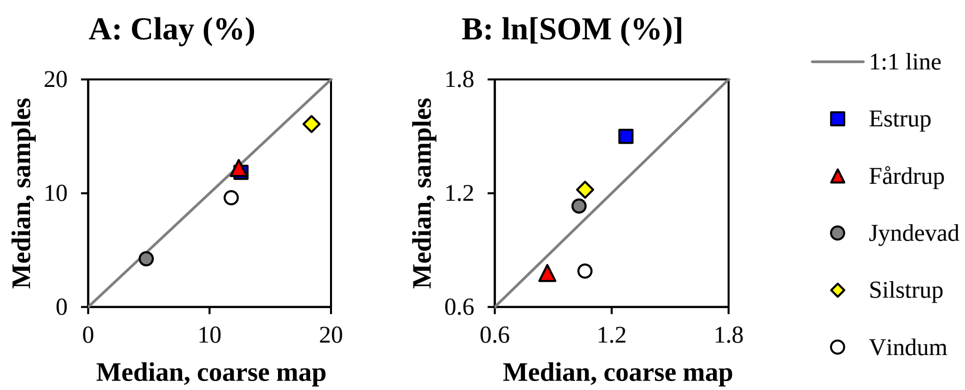

Figure 3: Median measured contents of (A) clay (<2 µm, % weight of mineral fraction) and (B) natural logarithmic soil organic matter (ln[SOM]) in the five fields included in the study relative to the median values of the fields in the coarse-resolution maps (Adhikari et al., 2013, Adhikari et al., 2014). Grey lines represent the 1:1 line.

3.2 Clay predictions

LR and LOESS generally predicted similar relationships between clay contents and EC (Figure 4). A notable difference is that LOESS predicted lower clay contents at low EC for Silstrup. Another difference is the wider prediction interval of LOESS at high EC at Vindum.

The predicted relationships between clay contents and EC also generally matched the observed relationships. The main difference is the positive bias of the predictions at Silstrup and Vindum. The bias in the coarse-resolution map for these fields is the most likely cause of this prediction bias. Furthermore, the observed clay contents at Jyndevad show no trend in their relationship with EC. This is attributable to the low clay contents of the soil, compared to the other fields, but both LR and LOESS still predicted a slight positive trend.

Moreover, in all fields except Vindum, all observations were within the 95% prediction interval, for LR as well as LOESS.

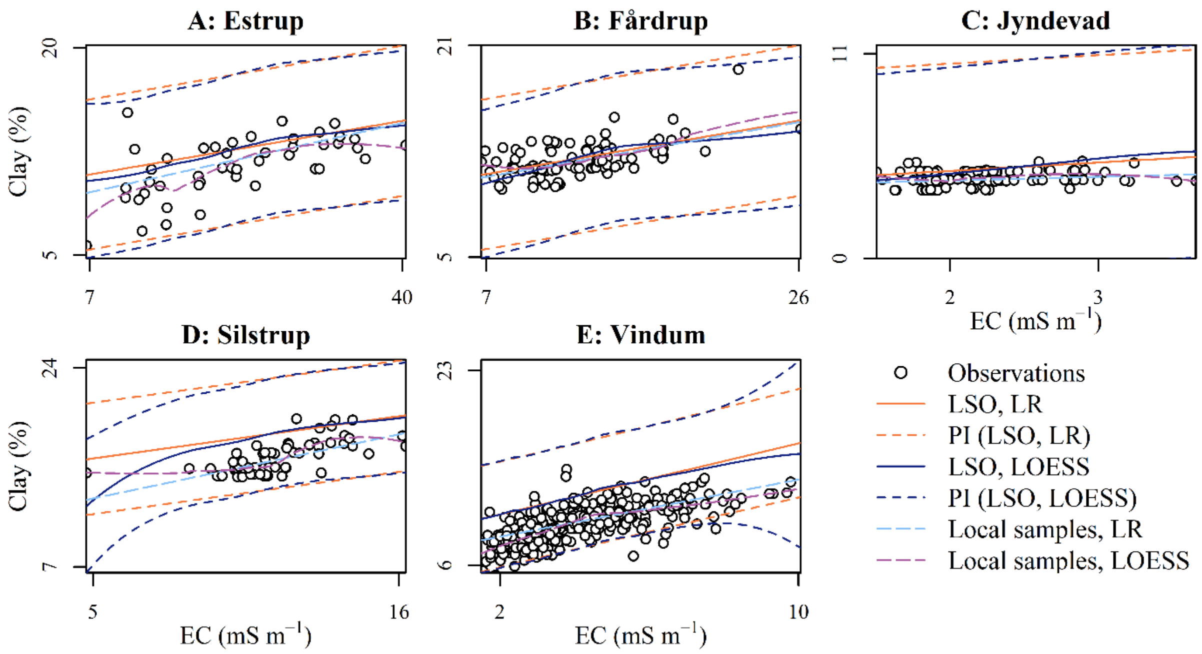

Figure 4: Predicted and observed relationships between clay contents and EC (0 – 30 cm) for the five fields. Each plot shows the relationship predicted with linear regression (LR) and local regression (LOESS). For both regression types, the plots show predictions using local samples as well as leave-site-out (LSO) predictions. Furthermore, the plots show the 95% prediction intervals (PI) for LSO predictions. Figure 10 shows the accuracies of the predictions.

The maps of clay contents produced with LR (Figure 5) and LOESS (Figure 6) are also very similar. At Silstrup, LOESS predicted lower clay contents than LR for a small area in the northern part of the field. In addition, LOESS predicted lower maximum clay contents than LR at Estrup, Silstrup and Vindum. However, the differences are generally small.

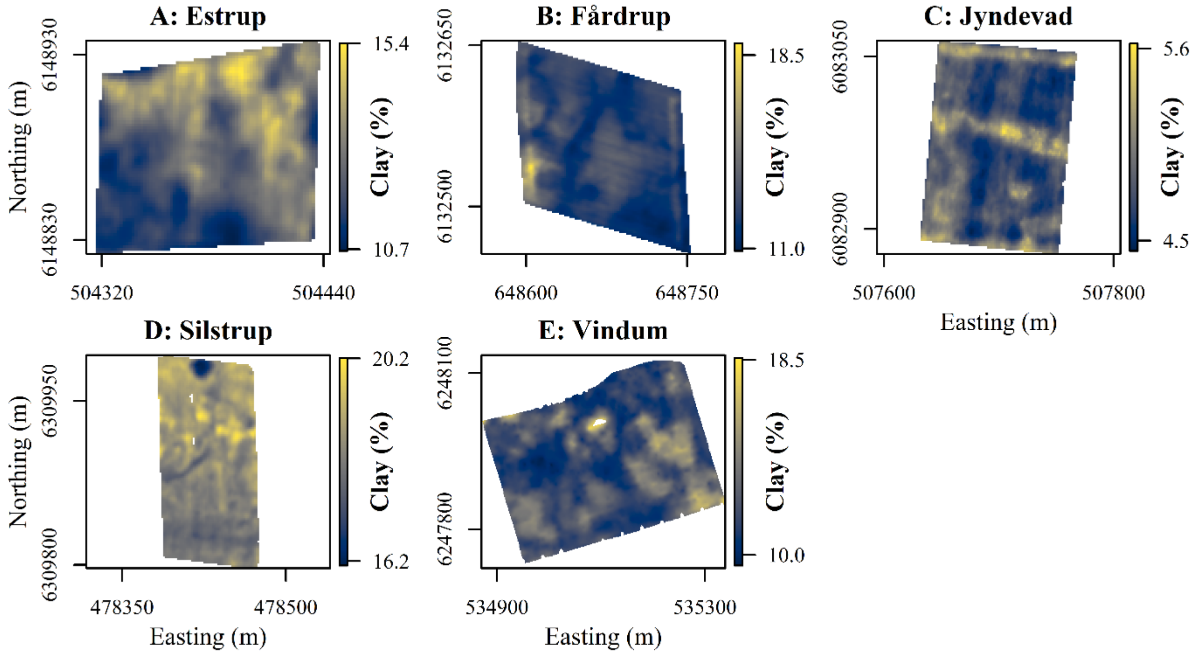

Figure 5: Maps of leave-site-out (LSO) predictions of clay contents for each field with linear regression (LR). The axes show coordinates for UTM zone 32N, ETRS 1989.

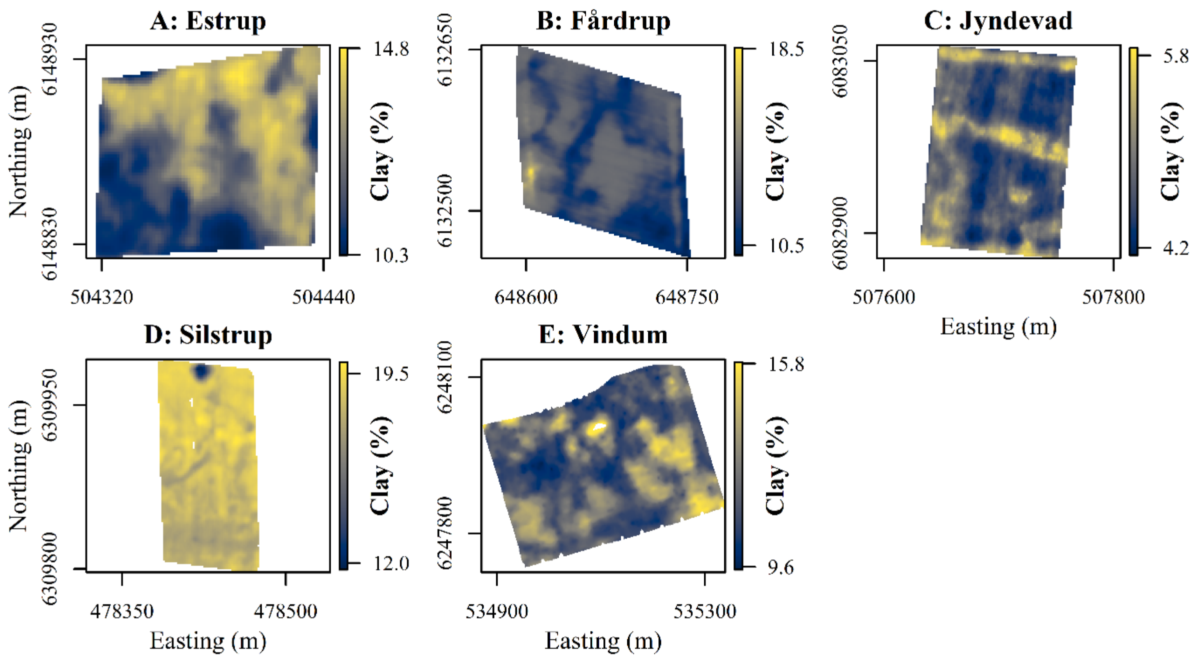

Figure 6: Maps of leave-site-out (LSO) predictions of clay contents for each field with local regression (LOESS). The axes show coordinates for UTM zone 32N, ETRS 1989.

3.3 SOM predictions

LR and LOESS predicted different relationships between SB and SOM (Figure 7). The observed relationships were non-linear. As a result, at Estrup, Jyndevad and Silstrup, LR predicted SOM contents that were lower than observed values for areas with high SB. At Vindum, for areas with low SB, both LR and LOESS predicted SOM contents that were lower than observed values, but the difference was largest for LR. At Fårdrup and Jyndevad, LR predicted SOM contents at low SB that were higher than observed values.

LOESS matched observed patterns more closely than LR. The only clear deviation from the observed patterns is the systematically low SOM prediction at Silstrup. The negative bias for Silstrup in the coarse-resolution map is the most likely cause of this deviation (Figure 3). However, Estrup and Vindum also had large biases in the coarse-resolution map without similar effects on the predictions.

At Vindum, some observations were outside the 95% prediction interval, but at Estrup, Fårdrup, Jyndevad and Silstrup, all observations were within the prediction intervals of both regression types.

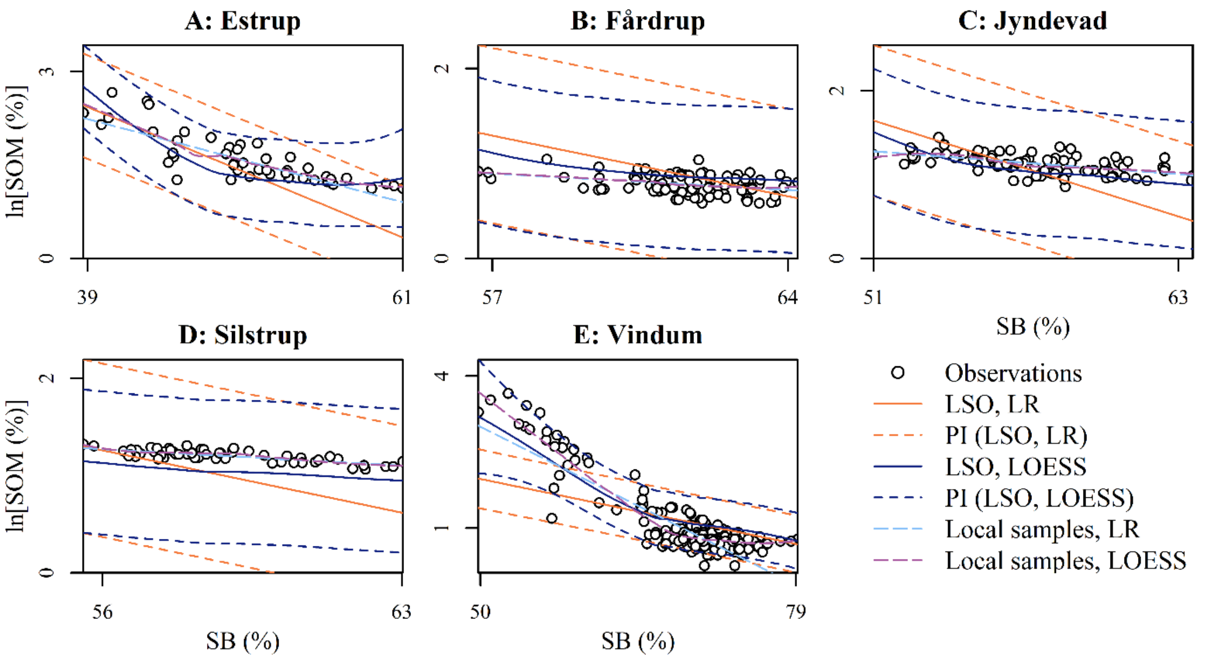

Figure 7: Predicted and observed relationships between natural-logarithmic transformed soil organic matter contents (ln[SOM]) and soil brightness (SB) in the red band for the five fields. Each plot shows the relationship predicted with linear regression (LR) and local regression (LOESS). For both regression types, the plots show predictions using local samples as well as leave-site-out (LSO) predictions. Furthermore, the plots show the 95% prediction intervals (PI) for LSO predictions. Figure 10 shows the accuracies of the predictions.

At Fårdrup, Jyndevad and Silstrup, LR and LOESS generally predicted similar SOM contents, in terms of patterns and range (Figure 8, Figure 9). However, in all three fields, LOESS generally concentrated high SOM predictions in smaller areas than LR. Furthermore, the maximum SOM contents predicted with LOESS were higher than the maximum SOM contents predicted with LR at Estrup and Vindum. This is especially clear at Vindum, where the highest SOM contents predicted by LOESS were more than five times larger than the highest SOM contents predicted with LR. Estrup and Vindum had the highest observed and predicted maximum SOM contents.

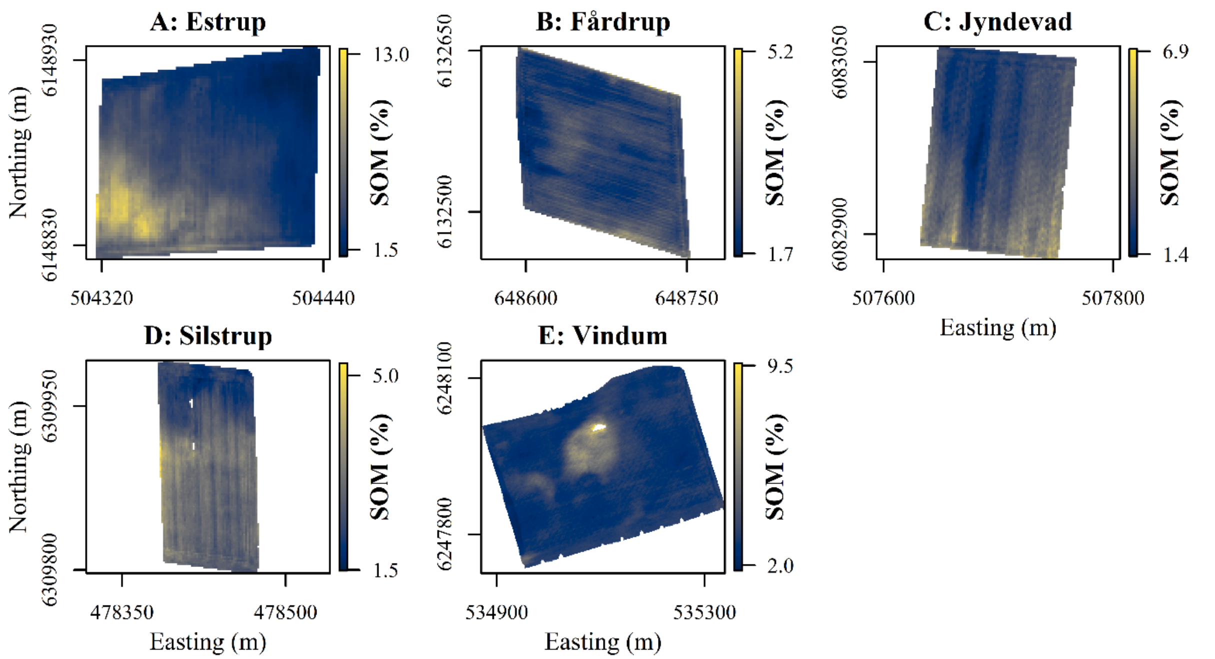

Figure 8: Maps of the leave-site-out (LSO) predictions of soil organic matter (SOM) contents for each field with linear regression (LR). The axes show coordinates for UTM zone 32N, ETRS 1989.

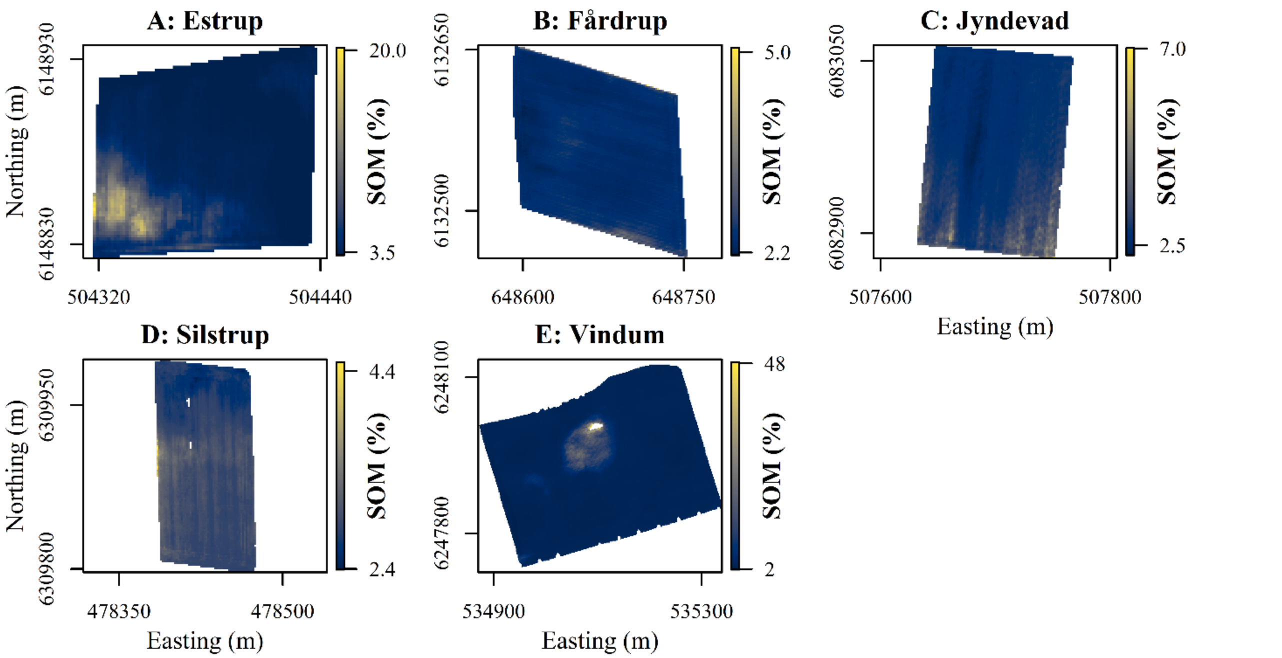

Figure 9: Maps of the leave-site-out (LSO) predictions of soil organic matter (SOM) contents for each field with local regression (LOESS). The axes show coordinates for UTM zone 32N, ETRS 1989.

3.4 Predictive accuracy

R^2 for the coarse-resolution maps was generally low, with a maximum of 0.31 for clay contents at Silstrup (Figure 10). R^2 for LSO predictions was generally higher, and in most cases, it was on par with the R^2 of predictions with local samples. For clay contents, the R^2 of LSO predictions ranged from 0.04 at Jyndevad (LR) to 0.48 at Vindum (LOESS). For SOM contents, the R^2 of LSO predictions ranged from 0.11 at Fårdrup (LOESS) to 0.88 at Vindum (LOESS). The mean R^2 for LSO predictions of clay contents was highest for LR (0.33 versus 0.29), but for SOM contents, it was similar for LR and LOESS (0.49 and 0.48, respectively).

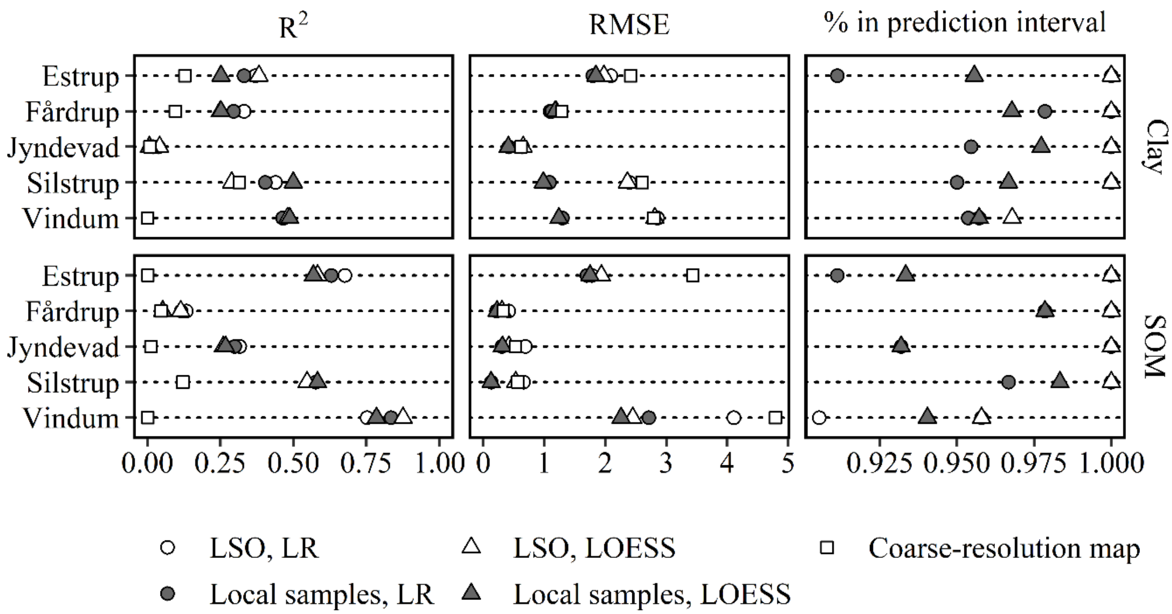

Figure 10: Accuracy of the predictions of clay and soil organic matter (SOM) contents for each field, calculated as Pearson's R^2 and root mean square error (RMSE), as well as the percentage of observations in the 95% prediction interval. The figure shows accuracies of predictions with linear regression (LR) and local regression (LOESS). For both regression types, the figure shows accuracies for leave-site-out (LSO) predictions and predictions with local samples. It also shows

the accuracies of the coarse-resolution maps. The coarse-resolution maps have no prediction intervals.

The RMSE for the coarse-resolution maps was highly variable. For clay contents, the RMSE of the coarse-resolution map varied from 0.6 at Jyndevad to 2.8 at Vindum, and for SOM contents, it varied from 0.3 at Fårdrup to 4.8 at Vindum. The RMSE of the LSO predictions was generally lower than the RMSE of the coarse-resolution maps. For clay contents, it varied from 0.6 at Jyndevad (LR) to 2.9 at Vindum (LR). For SOM contents, it varied from 0.3 at Fårdrup (LOESS) to 4.1 at Vindum (LR). The mean RMSE of the LSO predictions of clay contents was similar for LR and LOESS (1.8 for both), but for SOM contents, it was lowest for LOESS (1.1 versus 1.5). As LR yielded a higher R^2 than LOESS for clay contents (0.33 versus 0.29), we decided to use LR for this purpose. Furthermore, the behavior of LR was more robust than the behavior of LOESS. However, for SOM contents, the RMSE of the LSO predictions was lowest for LOESS, and we therefore decided to use LOESS for this purpose. LOESS generally predicted the non-linear behavior of ln[SOM] more closely than LR.

For clay contents predicted with LR, relative improvement (RI) in RMSE was large at Estrup (70%) and Fårdrup (116%), but low at Jyndevad (-12%), Silstrup (15%) and Vindum (-1%). The mean RI for clay contents was 38%. For SOM contents predicted with LOESS, RI was high at Estrup (95%) and Vindum (92%), moderate at Jyndevad (49%) and low at Fårdrup (19%) and Silstrup (8%). The mean RI for SOM was 53%. Therefore, in the best cases, the RMSE of the LSO predictions was on par with the RMSE of predictions with local samples. However, in the worst cases, the RMSE of LSO predictions was higher than the RMSE of the coarse-resolution maps. The results therefore only partially confirm Hypothesis 1, which stated that the LSO predictions would be more accurate than the coarse-resolution maps.

The prediction intervals were generally wider than expected, as the 95% prediction intervals contained 100% of the observations for all fields except Vindum. LR predictions of SOM for Vindum were the only case where the 95% prediction intervals contained less than 95% of the data. The results therefore reject Hypothesis 2, which stated that it was possible to estimate accurately the uncertainties related to the method.

3.5 Validity of assumptions

The first assumption, that the median values in the coarse-resolution maps represented accurately the observed medians, was generally true (Figure 3). Moreover, the validity of this assumption had a large impact on the accuracy of the predictions. Deviations from the observed median in the coarse-resolution maps created clear biases in the predictions. Such biases were clear in the clay contents predicted at Silstrup and Vindum (Figure 4) and the SOM contents predicted at Silstrup (Figure 7).

Correlation between EC and clay contents was moderate (R^2 = 0.33 – 0.47) for most fields except Jyndevad, where it was low (R^2 = 0.04). The assumption that clay contents were the main driver of variation in EC for each field was therefore moderately true. Moreover, Jyndevad had both the lowest R^2 and the smallest RI, most likely due to its low clay contents, which give a low SNR. This shows that good correlation between EC and clay contents is necessary in order to predict clay contents accurately with this method.

Correlation between ln[SOM] and SB was low at Fårdrup (R^2 = 0.13), but moderate to high for the other fields (R^2 = 0.31 – 0.75). The assumption that SOM in the main driver of variation in SB within each field is therefore generally true. In addition, Estrup and Vindum had the highest correlation between ln[SOM] and SB (R^2 = 0.68 and 0.75, respectively) and the highest RIs (95% and 92%, respectively), while Fårdrup had the lowest R^2 and a low RI. This shows that a high correlation between SOM and SB was important in order to predict SOM contents accurately.

The results therefore confirm Hypothesis 3, which stated the fulfillment of the three assumptions listed in the introduction would be the deciding criterion for the accuracy of the LSO predictions.

3.6 Effect of inverting EMI measurements

In this study, we used inverted EMI measurements for the depth interval 0 to 30 cm. We did this to obtain the EC only for the topsoil and to remove effects from soil properties at larger depths. Inversion should therefore improve the correlation between EC and clay contents in the topsoil. The results of our study shows that the correlation between clay contents and EC has a large impact on the accuracy of predicted clay contents. We therefore tested the assumption that inversion improved correlation by comparing correlation between clay contents and EC, as well as correlation between clay contents and EC_a of the individual DUALEM channels (Table 2).

Table 2: Pearson's R^2 for the correlation between observed clay contents, EC and EC_a. The table lists R^2 for EC for the depth interval 0 to 30 cm as well as EC_a measured by each of the four DUALEM channels.

	EC	**EC_a**			
Field	**0 - 30 cm**	**1mPRP**	**1mHCP**	**2mPRP**	**2mHCP**
Estrup	0.37	0.32	0.24	0.26	0.17
Fårdrup	0.33	0.28	0.25	0.23	0.15
Jyndevad	0.04	0.04	0.02	0.00	0.01
Silstrup	0.44	0.31	0.34	0.23	0.03
Vindum	0.47	0.56	0.56	0.53	0.47

The comparison shows that R^2 for EC was higher than R^2 for EC_a in any of the individual DUALEM channels except for Vindum. At Vindum, R^2 for EC was lower than R^2 for EC_a in any of the individual DUALEM channels. This is partly because of the smoothing of the data using a larger running mean width to improve the SNR before performing the inversion routine. However, despite this fact, even for EC, Vindum had a higher R^2 than the four other fields. As inverted data yielded higher correlations for most fields, we recommend that researchers use inverted EMI measurements for the method proposed in this study.

3.7 Possible improvements

The most obvious need for improvement to the method used in this study is a better way to estimate the uncertainties of the predictions. The prediction intervals were almost universally too wide. It is possible that a non-parametric method of uncertainty estimation, such as bootstrapping, would provide more accurate prediction intervals. The computational simplicity of the method would make it very straightforward to carry out a large number of repetitions from bootstrap samples of the soil observations from each field and use these repetitions to estimate uncertainties. Preferably, each of these repetitions should recalculate the median of the observations, in order to account for uncertainties in the median values, in addition to the uncertainty of the trend.

It is also a question if the coarse-resolution maps present systematic biases in the median values for the fields. Figure 3 suggest that this may be the case. It appears that the median clay contents in the coarse-resolution map are systematically higher than the observed medians, especially at higher clay contents. It also appears that the median SOM contents are higher than observed values for fields with low SOM contents and lower than observed values for fields with high SOM contents. However, the number of fields is too low for one to assess if these biases are truly systematic or if it is a spurious relationship.

In this study, we used only existing data and therefore selected the five fields based on data availability. The number and representability of the fields therefore constitute limitations. The first limitation is the relatively small number of fields. The current number is adequate for a first test of the method. However, although the improvements in accuracy are in most cases promising, it is still possible that the results constitute a “lucky shot” with the current number of fields. Furthermore, the current approach is relatively simple, and in order to develop a more advanced approach, a larger number of fields would be necessary. The second limitation is the representability of the results for SOM. We only used fields with predominantly mineral topsoils. Estrup and Vindum had small areas with organic topsoils, but mineral topsoils dominated all five fields. It is therefore a question how well the method used in this study will work for fields with predominant organic topsoils. It is likely that the method will need alterations to work for this purpose, and the accuracy of the predictions will likely depend on whether or not the coarse-resolution maps correctly predict the mineral or organic nature of the topsoil. With these limitations in mind, it should also be possible to use the proposed method to map additional soil properties in addition to clay and SOM contents. For example, soil salinity also correlates with EC_a (Corwin and Lesch, 2005), and in arid and semi-arid areas, the purpose of the method could instead be to map soil salinity at field level. In this case, the use of the method would require large extent maps of soil salinity as an input, in order to adjust median salinity. Furthermore, the method for mapping SOM could rely on additional sources of imagery in addition to aerial imagery. If no bare-soil aerial imagery is immediately available, soil mappers could instead use drone imagery or high-resolution satellite imagery, for example from the Sentinel 2 mission (European Space Agency, n.d.).

In this study, bias in the median values of the coarse-resolution map generally imposed a clear limitation on the accuracy of the predictions. Therefore, a way to increase the accuracy of the predictions would be to use coarse-resolution maps with higher accuracies. Methods for digital soil mapping constantly develop, and it is likely that future coarse-resolution maps will be more accurate. Even if a new map does not account for intra-field variability more accurately than the previous map, a more accurate median value would increase the accuracy of predictions with the method used in this study.

4 Conclusions

In this study, we present a method to predict clay and SOM contents from EMI and aerial imagery without the use of local samples. We tested the method for five agricultural fields in Denmark and found that the method generally, but not universally, provided more accurate results than national-level, coarse-resolution maps. The improvements were largest and most consistent for SOM predictions, especially for fields with large ranges in SOM contents. Linear regression (LR) generally predicted clay contents most accurately, while local regression (LOESS) generally predicted SOM contents most accurately. Methods for estimating the uncertainties of the method need further refinement, as prediction intervals were generally too wide. However, as it is, the method constitutes a simple and reliable tool for estimating clay and SOM contents within agricultural fields. This can be useful for situations when no local data are available, for example when planning sampling designs, or screening for constraints to agricultural land uses or environmental threats. Although soil surveyors may be skilled at interpreting EMI data and aerial imagery, being able to provide a quantitative estimate, instead of a relative estimate, greatly increases the usefulness of these data.

5 Code and data availability

The data and R code used in the study are available at https://doi.org/10.5281/zenodo.3699130.

6 Author contribution

All authors collaborated to the design of the study. Anders Bjørn Møller prepared the data, and Triven Koganti carried out inversion of EMI data. Anders Bjørn Møller carried out the analyses and prepared the manuscript with inputs from all authors.

7 Competing interests

The authors declare that they have no conflict of interest.

8 Acknowledgements

The authors are obliged to Cecilie Hermansen, who helped compiling the data.

References

Achasov, A.B. and Bidolakh, D.I., 2011. The use of space and ground digital photography for determining the humus content in soils. Eurasian Soil Sci. 41(3), 249-254. http://dx.doi.org/10.1134/s1064229308030022.

Adhikari, K., Hartemink, A.E., Minasny, B., Kheir, R.B., Greve, M.B. and Greve, M.H., 2014. Digital mapping of soil organic carbon contents and stocks in Denmark. PLOS ONE 9(8), e105519. http://dx.doi.org/10.1371/journal.pone.0105519.

Adhikari, K., Kheir, R.B., Greve, M.B., Bøcher, P.K., Malone, B.P., Minasny, B., McBratney, A.B. and Greve, M.H., 2013. High-resolution 3-D mapping of soil texture in Denmark. Soil Sci. Soc. Am. J. 77(3), 860-876. http://dx.doi.org/10.2136/sssaj2012.0275.

Agency for Data Supply and Efficiency. 2019. GeoDanmark. https://sdfe.dk/hent-data/fotos-og-geodanmark-data/ (accessed 26-08-19).

Auken, E., Christiansen, A.V., Kirkegaard, C., Fiandaca, G., Schamper, C., Behroozmand, A.A., Binley, A., Nielsen, E., Effersø, F., Christensen, N.B., Sørensen, K., Foged, N. and Vignoli, G., 2015. An overview of a highly versatile forward and stable inverse algorithm for airborne, ground-based and borehole electromagnetic and electric data. Explor. Geophys. 46(3), 223-235. http://dx.doi.org/10.1071/eg13097.

Auken, E., Viezzoli, A. and Christensen, A., 2009. A single software for processing, inversion, and presentation of AEM data of different systems: the Aarhus Workbench. ASEG Ext. Abstr. 2009(1), 1. http://dx.doi.org/10.1071/ASEG2009ab062.

Callegary, J.B., Ferré, T.P.A. and Groom, R.W., 2007. Vertical spatial sensitivity and exploration depth of low-induction-number electromagnetic-induction instruments. Vadose Zone J. 6(1), 158. http://dx.doi.org/10.2136/vzj2006.0120.

Chen, F., Kissel, D.E., West, L.T. and Adkins, W., 2000. Field-scale mapping of surface soil organic carbon using remotely sensed imagery. Soil Sci. Soc. Am. J. 64(2), 746-753. http://dx.doi.org/10.2136/sssaj2000.642746x.

Christiansen, A.V., Pedersen, J.B., Auken, E., Soe, N.E., Holst, M.K. and Kristiansen, S.M., 2016. Improved geoarchaeological mapping with electromagnetic induction instruments from dedicated processing and inversion. Remote Sens. 8(12), 1022. http://dx.doi.org/10.3390/rs8121022.

Cleveland, W., Grosse, E. and Shyu, W., 1992. Local regression models, in: Chambers, J.M. and Hastie, T.J. (Eds.), Statistical models in S. Chapman & Hall, New York, 309 - 376.

Corwin, D.L. and Lesch, S.M., 2005. Apparent soil electrical conductivity measurements in agriculture. Comput. Electron. Agric. 46(1-3), 11-43. http://dx.doi.org/10.1016/j.compag.2004.10.005.

Corwin, D.L. and Rhoades, J.D., 1982. An improved technique for determining soil electrical conductivity-depth relations from above-ground electromagnetic measurements. Soil Sci. Soc. Am. J. 46(3), 517. http://dx.doi.org/10.2136/sssaj1982.03615995004600030014x.

Doolittle, J.A. and Brevik, E.C., 2014. The use of electromagnetic induction techniques in soils studies. Geoderma 223-225, 33-45. http://dx.doi.org/10.1016/j.geoderma.2014.01.027.

Dualem Inc, 2007. Dualem-21S User's Manual, Dualem Inc., Milton.

European Space Agency. n.d. Missions: Sentinel-2. https://sentinel.esa.int/web/sentinel/missions/sentinel-2 (accessed 14-12-16).

Everett, M.E., 2013. Electromagnetic induction, in: Near-surface applied geophysics. Cambridge University Press, 200-238.

Fox, G.A. and Sabbagh, G.J., 2002. Estimation of soil organic matter from red and near-infrared remotely sensed data using a soil line Euclidean distance technique. Soil Sci. Soc. Am. J. 66(6), 1922-1929. http://dx.doi.org/10.2136/sssaj2002.1922.

Gee, G.W. and Bauder, J.W., 1986. Particle-size analysis, in: Klute, A. (Ed.) Methods of soil analysis: Part 1 Physical and mineralogical methods. 5, 383-411.

Gelder, B.K., Anex, R.P., Kaspar, T.C., Sauer, T.J. and Karlen, D.L., 2011. Estimating soil organic carbon in central Iowa using aerial imagery and soil surveys. Soil Sci. Soc. Am. J. 75(5), 1821-1828. http://dx.doi.org/10.2136/sssaj2010.0260.

Greve, M.H., Christensen, O.F., Greve, M.B. and Kheir, R.B., 2014. Change in peat coverage in Danish cultivated soils during the past 35 years. Soil Sci. 179(5), 250-257. http://dx.doi.org/10.1097/ss.0000000000000066.

Greve, M.H. and Greve, M.B., 2004. Determining and representing width of soil boundaries using electrical conductivity and MultiGrid. Comput. Geosci. 30(6), 569-578. http://dx.doi.org/10.1016/j.cageo.2004.01.005.

Heil, K. and Schmidhalter, U., 2012. Characterisation of soil texture variability using the apparent soil electrical conductivity at a highly variable site. Comput. Geosci. 39, 98-110. http://dx.doi.org/10.1016/j.cageo.2011.06.017.

Heil, K. and Schmidhalter, U., 2017. The application of EM38: Determination of soil parameters, selection of soil sampling points and use in agriculture and archaeology. Sensors (Basel) 17(11). http://dx.doi.org/10.3390/s17112540.

Khongnawang, T., Zare, E., Zhao, D., Srihabun, P. and Triantafilis, J., 2019. Three-dimensional mapping of clay and cation exchange capacity of sandy and infertile soil using EM38 and inversion software. Sensors (Basel) 19(18). http://dx.doi.org/10.3390/s19183936.

Koganti, T., Narjary, B., Zare, E., Pathan, A.L., Huang, J. and Triantafilis, J., 2018. Quantitative mapping of soil salinity using the DUALEM-21S instrument and EM inversion software. Land Degrad. Dev. 29(6), 1768-1781. http://dx.doi.org/10.1002/ldr.2973.

Ladoni, M., Bahrami, H.A., Alavipanah, S.K. and Norouzi, A.A., 2009. Estimating soil organic carbon from soil reflectance: A review. Precis. Agric. 11(1), 82-99. http://dx.doi.org/10.1007/s11119-009-9123-3.

Lindhardt, B., Abildtrup, C., Vosgerau, H., Olsen, P., Torp, S., Iversen, B.V., Jørgensen, J.O., Plauborg, F., Rasmussen, P. and Gravesen, P., 2001. The Danish pesticide leaching assessment programme. Site characterization and monitoring design. Geological Survey of Denmark and Greenland, Copenhagen, Denmark.

Madsen, H.B. and Jensen, N.H., 1985. The establishment of pedological soil data bases in Denmark. Dan. J. Geogr. 85(1), 1-8. http://dx.doi.org/10.1080/00167223.1985.10649211.

Madsen, H.B., Nørr, A.H. and Holst, K.A., 1992. The Danish soil classification. The Royal Danish Geographical Society, Copenhagen, Denmark.

Magri, A., Van Es, H.M., Glos, M.A. and Cox, W.J., 2005. Soil test, aerial image and yield data as inputs for site-specific fertility and hybrid management under maize. Precis. Agric. 6(1), 87-110. http://dx.doi.org/10.1007/s11119-004-0687-7.

McNeill, J.D., 1980. Electromagnetic terrain conductivity measurement at low induction numbers.

Michael Mertens, F., Pätzold, S. and Welp, G., 2008. Spatial heterogeneity of soil properties and its mapping with apparent electrical conductivity. J. Plant Nutr. Soil Sci. 171(2), 146-154. http://dx.doi.org/10.1002/jpln.200625130.

Møller, A.B., Beucher, A.M., Pouladi, N. and Greve, M.H., 2019. Oblique geographic coordinates as covariates for digital soil mapping. SOIL Discuss. http://dx.doi.org/10.5194/soil-2019-83.

Olesen, S. and Simmelsgaard, S., 1995. Danish research on site specific farming. Site Specific Farming, 20-21 Mar 1995, Aarhus, Denmark, SP.

Pouladi, N., Møller, A.B., Tabatabai, S. and Greve, M.H., 2019. Mapping soil organic matter contents at field level with Cubist, Random Forest and kriging. Geoderma 342, 85-92. http://dx.doi.org/10.1016/j.geoderma.2019.02.019.

Roberts, D.F., Adamchuk, V.I., Shanahan, J.F., Ferguson, R.B. and Schepers, J.S., 2010. Estimation of surface soil organic matter using a ground-based active sensor and aerial imagery. Precis. Agric. 12(1), 82-102. http://dx.doi.org/10.1007/s11119-010-9158-5.

Tabatabai, M.A. and Bremner, J.M., 1970. Use of the Leco automatic 70-second carbon analyzer for total carbon analysis of soils. Soil Sci. Soc. Am. J. 34(4), 608-610. http://dx.doi.org/10.2136/sssaj1970.03615995003400040020x.

Triantafilis, J. and Lesch, S.M., 2005. Mapping clay content variation using electromagnetic induction techniques. Comput. Electron. Agric. 46(1-3), 203-237. http://dx.doi.org/10.1016/j.compag.2004.11.006.

Varvel, G.E., Schlemmer, M.R. and Schepers, J.S., 1999. Relationship between spectral data from an aerial image and soil organic matter and phosphorus levels. Precis. Agric. 1(3), 291-300. http://dx.doi.org/10.1023/a:1009973008521.

Viezzoli, A., Christiansen, A.V., Auken, E. and Sørensen, K., 2008. Quasi-3D modeling of airborne TEM data by spatially constrained inversion. Geophys. 73(3), F105-F113. http://dx.doi.org/10.1190/1.2895521.

Williams, B.G. and Baker, G.C., 1982. An electromagnetic induction technique for reconnaissance surveys of soil salinity hazards. Soil Res. 20(2), 107. http://dx.doi.org/10.1071/sr9820107.

Williams, B.G. and Hoey, D., 1987. The use of electromagnetic induction to detect the spatial variability of the salt and clay contents of soils. Aust. J. Soil Res. 25(1), 21-27. http://dx.doi.org/10.1071/Sr9870021.

Wollenhaupt, N.C., Richardson, J.L., Foss, J.E. and Doll, E.C., 1986. A rapid method for estimating weighted soil salinity from apparent soil electrical conductivity measured with an aboveground electromagnetic induction meter. Can. J. Soil Sci. 66(2), 315-321. http://dx.doi.org/10.4141/cjss86-032.

Wu, C.W., Xia, J.X., Yang, H., Yang, Y., Zhang, Y.C. and Cheng, F.W., 2018. Rapid determination of soil organic matter content based on soil colour obtained by a digital camera. Int. J. Remote Sens. 39(20), 6557-6571. http://dx.doi.org/10.1080/01431161.2018.1460511.